NASA TM X-448

TECHNICAL MEMORANDUM

X-448

INVESTIGATION OF THE CHARACTERISTICS OF 6-FOOT DROGUE-STABILIZATION RIBBON PARACHUTES AT HIGH ALTITUDES AND LOW SUPERSONIC SPEEDS

By Clinton T. Johnson

Flight Research Center
Edwards, Calif.

NATIONAL AERONAUTICS AND SPACE ADMINISTRATION
WASHINGTON
November 1960

CONFIDENTIAL

NATIONAL AERONAUTICS AND SPACE ADMINISTRATION

TECHNICAL MEMORANDUM X-448

INVESTIGATION OF THE CHARACTERISTICS OF 6-FOOT DROGUE-STABILIZATION RIBBON PARACHUTES AT HIGH ALTITUDES AND LOW SUPERSONIC SPEEDS*

By Clinton T. Johnson

SUMMARY

Performance data are presented for two types of ribbon parachutes. The parachutes were forcibly deployed from an air-launched test vehicle at altitudes from 55,000 feet to 70,000 feet and at Mach numbers between 0.92 and 1.52. Opening shock, steady-state drag performance, and canopy-porosity effects are evaluated with respect to Mach number and dynamic pressure.

The conical canopy design appears to function far better than the flat canopy at supersonic deployment speeds. The relatively high-porosity conical design improves the parachute stability, with the added benefit of a low opening shock. The drag efficiency of the conical canopy is equivalent to that of the flat canopy having 50-percent-lower porosity. Riser elasticity and length also appear to be important parameters affecting the parachute stability. Reducing the weight of the test vehicle by a factor of one-third had a negligible effect on the stability and drag characteristics of the parachute.

Canopy overinflation occurred for all supersonic tests and produced an oscillating load frequency of about 30 to 40 cycles per second with a fluctuating load of approximately ±200 pounds. The data showed that the oscillations ceased at a Mach number of about 1.14.

Comparison with data from subsonic sled tests indicates pronounced Mach number effects on opening shock and inflated drag coefficients.

Packaging the canopy and riser in a specially designed deployment bag and forcibly expelling the bag from a mortar with an explosive charge proved to be a reliable method of insuring proper canopy deployment.

*Title, Unclassified.

INTRODUCTION

Use of ribbon-type drogue parachutes has been proposed for stabilizing blunt bodies reentering the atmosphere from orbit. The altitudes and Mach numbers at which such parachutes would be deployed are in the flight regime where parachute technology is not fully developed. Thus, when a drogue parachute was incorporated as a part of the recovery system for the Project Mercury manned capsule, extensive development work was required. Both wind-tunnel tests (ref. 1) and free-flight tests were made.

The primary objectives of the flight tests were to develop a ribbon-parachute canopy and riser combination with a low opening shock, an acceptable degree of stability, and minimum packed weight commensurate with strength requirements. Previous tests with ribbon-type parachutes indicated that canopy-filling time, opening shock, and inflated drag characteristics were largely unknowns at high altitudes and supersonic speeds. The requirement for a long riser introduced another variable for which free-flight data were generally unavailable. Forcible canopy deployment was necessary at these speeds. This technique introduced inertial forces that could possibly exceed other transient loads.

The free-flight tests were conducted at the NASA Flight Research Center, Edwards, Calif. An air-launch technique was used to deploy the test parachutes at altitudes and Mach numbers which would simulate the final reentry conditions of the Project Mercury capsule. Instrumented test vehicles were launched over a precision-bombing range equipped with radar and Askania tracking coverage. Results from these flight tests are described herein.

SYMBOLS

C_D	drag coefficient, F/qS
F	drag force, lb
h_p	altitude, ft
M	Mach number
q	dynamic pressure, $\frac{1}{2}\rho V^2$, lb/sq ft
S	projected area of canopy based on constructed diameter of canopy (28.3 sq ft), sq ft

V	velocity, ft/sec
λ_g	constructed porosity of ribbon canopy expressed in percent (ratio of the area of the drag-producing surface not covered by ribbons to the total drag-producing area)
ρ	standard ARDC density, slugs/cu ft

Subscripts:

i	inflated
o	opening-shock condition of canopy
s	conditions at the time of snatch force

Standard parachute terminology is used as defined in the USAF parachute handbook (ref. 2).

DESCRIPTION OF APPARATUS

Parachute Configuration

The development testing program necessitated changes in several major parachute-design parameters before an acceptable configuration was found. Table I presents a summary of the parameters and the order in which they were tested. Initially, ribbon parachutes of standard flat design and nominal 6-foot diameter were selected for testing on the basis of existing parachute technology and availability of the flat-canopy design with several porosities. A second type of canopy having a shaped-conical design was subsequently adopted to obtain improved stability. Dynamic instabilities of the canopy-riser combination also dictated a major change in the riser material during the later stages of the testing.

The flat-canopy design is constructed as a flat circular plate composed of concentric ribbons supported by heavy radial ribbons and small vertical tapes between the radial ribbons. Porosity is governed by the spacing of the concentric, or horizontal, ribbons. The design strength of the canopy is controlled by varying the strength of the ribbon material.

Figures 1(a) and 1(b) show photographs of two flat-design ribbon canopies incorporating extremes in the porosities tested. It should be noted that the 30-percent-porosity canopy was designed with 10 gores,

whereas all other test canopies were designed with 8 gores. The shroud lines were of 1/2-inch-wide, 6-foot-long, flat, tubular Nylon material rated at 1,000 pounds breaking strength. Shroud lines were overlap-sewn to the riser and secured with a waxed-cord serving. As a result of the loss of the first test canopy and evidence of severe fraying of the shroud lines at the confluence point on the second test, the individual shroud lines were wrapped with cotton material in subsequent tests to reduce the abrasive action between adjacent Nylon lines. Use of this technique solved the problem of confluence-point fraying arising from oscillatory motions of the test canopy.

The shaped-canopy designs are similar to the flat circular type, except that individual panels are shaped. The particular variation of the shaped canopy used in these tests was the 30° conical type. A photograph of a typical shaped canopy would show gore details similar to those of figure 1(b). The porosity of the conical canopy was 28 percent. All the details of the shroud lines and fastening were similar to those of the flat canopies.

A design feature common to all of the parachutes tested was the incorporation of pocket bands sewn to the skirt band at each radial ribbon. These pocket bands were designed to aid in initial canopy inflation and to serve as a device for maintaining a partially reefed condition of the canopy during the inflation process.

The riser length and types of material used in these tests were important variables. Unpublished wind-tunnel tests indicated that a canopy became more efficient when placed at least 5 body diameters behind the face of a bluff body. Consequently, risers varying from 30 to 40 feet in length were used to simulate the parachute rigging on the Project Mercury capsule. The material of which the riser was woven determined the elongation characteristics. Riser break strength was based on anticipated opening shock forces. Initial testing was done with 40-foot, single-layer, woven Nylon material of 6,000- and 9,000-pound break strength. Dynamic instabilities caused by the high elasticity of the Nylon riser necessitated changing to Dacron material with a lower elongation than Nylon. Later testing was conducted with Dacron which had undergone a "hot-stretch" process prior to weaving. This process substantially reduces the elasticity of regular Dacron. For the Dacron risers, the required strength was achieved by sewing together single layers of 3,000-pound break-strength material.

The test parachutes were forcibly deployed from a mortar installed in the parachute test vehicle. The canopies were hand packed into a deployment bag approximately 5 inches in diameter and 17 inches long. On most tests the entire riser was packed into the bag and bights were tied to loops inside the bag with break cord. The longer risers could not be completely stowed within the bag. Bag closure was accomplished

by tying the flaps with break cord which was, in turn, tied to the exposed riser. Each bag had a metal plate in the bottom for blast protection of the canopy. In addition, a few ounces of lead shot were sewn into the bottom of the bag to provide an additional inertia force for separation of the bag and packed canopy.

The packed canopy was fitted, bottom-first, into an aluminum sabot, and inserted sabot-first into the mortar. A rubber O-ring on the sabot made a pressure fit within the muzzle. A squib-ignited, 5-gram charge of black powder generated breech pressures sufficient to expel the sabot and packed chute with muzzle velocities of about 80 feet per second. The canopy and shroud lines weighed approximately 5 pounds.

Parachute Test Vehicle and Instrumentation

Photographs of the parachute test vehicle are presented in figures 2(a) and 2(b) which show, respectively, a side view of the aircraft and test-vehicle configuration, and a closeup of a mounted vehicle with details of attachment to the launch rail.

The vehicle consisted of a steel casing 14 inches in diameter and 67 inches long, with a 21-inch ogival-shape nose. Stability was provided by 7-inch-span cruciform fins. The test vehicle was ballasted with lead to a gross weight of approximately 1,500 pounds. The ogival nose was constructed of reinforced cast lead weighing approximately 700 pounds, with additional lead ballast cast in place in the casing.

Figure 3 presents some details of the load-supporting structure to which the riser was attached. Figure 3(a) shows the riser from the packed parachute, extending out of the mortar and attaching to the centerline-load structure. Figure 3(b) shows a centerline-mounted tensiometer with an off-center mortar. Figure 3(c) shows a partially assembled instrument capsule designed to be inserted into the test-vehicle casing. The capsule and casing were fastened together with explosive bolts placed through the mating flanges, as shown in figures 3(a) and 3(c). The load-support ring and the centerline-suspension point are shown in figure 3(c).

The test vehicles were fitted with rail-mating lugs (figs. 2(b) and 3(a)) which would allow the test vehicle to slide on the rail. A compressed-air piston on the launch rail was discharged, thus forcing the test vehicle to slide rearward about 2 inches before release. Emergency release could be effected by firing explosive bolts on the launch rail, which would release load-supporting segments of the launch rail.

Movie cameras were installed on the launch aircraft to qualitatively evaluate test-vehicle separation and parachute deployment. The cameras were mounted in the nose of the aircraft covering a field of view below and rearward of the nose. The cameras operated at 200 and 64 frames per second and were started by closure of microswitches as the launch rail was lowered by the supporting trapeze.

The test vehicles contained a system for operational sequencing of the vehicle components and a data-recording system. Prelaunch instrumentation power was supplied to the test vehicle through an umbilical cable. The test vehicles were broadly classified as noninstrumented, partially instrumented, and completely instrumented.

Noninstrumented test vehicle.- The vehicle was uninstrumented except for two movie cameras to provide qualitative evaluation of the test-parachute performance. These cameras, operating in sequence, recorded the deployment and opening at 100 frames per second and the remainder of the operation at 64 or 16 frames per second. A typical installation is shown in figure 3(a).

Partially instrumented test vehicle.- This vehicle was fitted with two movie cameras and a Coleman mechanical tensiometer to measure and record the canopy-riser forces (ref. 3). The tensiometer is a scratch-recorder device with an aluminum foil wrapped on a spring-wound, clockwork-driven drum. A stylus attached to a Belleville spring traced the force time history on the aluminum foil. An additional stylus driven by a battery-powered oscillator provided a time base on the aluminum foil. The tensiometer recorded data for approximately a 20-second period. The tensiometer clockwork was tripped by the pull on a light break cord attached to the riser. Figure 3(b) shows a tensiometer mounted in a partly assembled test vehicle.

Completely instrumented test vehicle.- Recorded on this vehicle were the canopy-riser force from a strain-gage tension link and the vehicle longitudinal acceleration. The vehicle also contained camera-framing synchronizers. Figure 3(c) shows a partially assembled instrument capsule, consisting of a movie camera, a load-release device on the end of the strain-gage tension link, and a universal joint for attachment of the tension link to the load-supporting structure. Also shown is the shock-mounted recording oscillograph.

Additional devices and instrumentation were provided on the test vehicles for starting cameras when the test vehicle was released, for igniting time-delay squibs (2 to 4 sec) to fire the mortar when the test vehicle was safely clear of the launch aircraft, and for transferring instrument power from the aircraft to the test vehicle at release. The instrument capsule was equipped with static-pressure sensors for firing the explosive bolts fastening the capsule to the

test-vehicle casing, and for firing the squib-loaded release device on the test parachute. The release of the test parachute extracted a large recovery parachute attached to the instrument capsule. When the recovery parachute was fully extracted, a lanyard released the pin of a CO_2-bottle used to inflate an impact bag attached to the base of the instrument capsule.

TEST PROCEDURE

Air-Launch Technique

An F-104A airplane was utilized as the launch aircraft for the parachute test vehicle. A hydraulically actuated trapeze mounted on the bottom of the fuselage was fitted with a missile-launching rail. When the trapeze was lowered, the rail was extended approximately $4\frac{1}{2}$ feet below the bottom of the fuselage. Launch-rail components were modified to provide positive and instantaneous release of the parachute test vehicle upon command of the pilot. Figures 2(a) and 2(b) show photographs of the test vehicle mounted on the launch aircraft.

The launch technique required precision radar vectoring of the aircraft to a preplanned point for initiating a zoom maneuver at an approximate constant climb angle. During the zoom, the bombing-range controller called out corrections required to reach the desired altitude and Mach number for release of the parachute test vehicle. Release was authorized by the bombing-range controller, based on range-safety considerations relative to a previously calculated impact point of the test vehicle. Studies of the zoom and launch procedures prior to the flight-test program indicated that a release-position error (translated into time at the planned release velocities and altitudes) greater than 5 seconds would impact the test vehicle, with a parachute malfunction, into a down-range danger area. A properly functioning parachute, on the other hand, could result in the vehicle falling into an up-range danger area. Azimuth errors greater than 2° would also exceed range-safety requirements.

Askania tracking cameras, spaced at intervals along each side of the precision-bombing range (approximately 14 miles long and 7 miles wide), provided data for subsequent trajectory analysis of the test-parachute performance. The Askania trackers also provided impact coverage for recovery of the instrumentation.

Test Conditions

The parachute test vehicle was released from the launch aircraft either in a level-flight condition at 1 g or at the peak of a zoom trajectory at approximately 0.5g. Test-vehicle separation was effected by means of a mechanical device on the launch rail.

The test conditions in terms of Mach number and altitude were selected in the general area of a possible reentry profile of the Project Mercury capsule. Figure 4 presents a summary of the canopy-deployment conditions at the various test altitudes. In addition to investigating the deployment and inflation characteristics of ribbon parachutes at low dynamic pressures and high altitudes, the parachutes were also proof-tested at dynamic pressures approximately 30 percent higher than design dynamic pressure. Canopy-deployment Mach number and altitude, presented in figure 4, vary, respectively, from $M = 0.92$ to $M = 1.52$ and from 71,100 feet to 54,500 feet.

ACCURACY OF DATA

Forces measured by the Coleman mechanical tensiometer have an accuracy of approximately ±8 percent of the applied load and ±0.10 second. Frequency response is flat to about 50 cycles per second. Reference 3 presents the results of an extensive investigation of this type of force-recording device. Recorded forces taken from the strain-gage tension link are believed to be accurate to within ±1 percent of the applied load.

The test-vehicle trajectory, velocity, and altitude were obtained from analysis of Askania tracking-camera data. Velocity is estimated to be accurate to within ±50 feet per second, and altitude to within ±500 feet. Calculated drag data, using the quantities derived from Askania trajectory data, correlated well with directly recorded canopy-riser forces. However, the use of Askania data to calculate the initial high, transient, canopy loads proved unreliable.

Data from the ARDC standard atmosphere tables were used to calculate Mach number and dynamic pressure. Errors arising from the use of standard conditions are estimated to result in errors of about 2 to 3 percent in the reduced data.

RESULTS AND DISCUSSION

Deployment and Inflation Characteristics

Canopy-opening process.- Parachute deployment and stability were qualitatively evaluated from moving pictures which were taken from the launch aircraft and from the parachute test vehicle. Typical installations on the test vehicles are shown in figures 3(a) and 3(c). The sequence of events, as indicated by the movies, occurring within 1 second after mortar firing is:

First, the packed canopy and riser are deployed as the mortar is fired. The bag generally tumbles as the riser is being payed out of the deployment bag, while the riser undergoes random movements. A snatch force develops as the packed canopy reaches the full extension of the riser, and, simultaneously, the deployment bag is stripped cleanly from the canopy.

The next sequence occurs as the deployed canopy begins inflating. The initial inflation is characterized by a rapid increase in diameter to the point where the opening shock occurs. After the opening shock, the canopy diameter decreases slightly and is accompanied by a reduction in the canopy-riser force. The canopy then begins to reinflate immediately with a more or less uniform increase in diameter, but is generally accompanied by unsymmetrical collapses of one or two gores of the canopy until it is fully inflated.

The final sequence of the opening process is the occurrence of a short period of canopy breathing, during which the canopy periodically overinflates. The breathing has an average frequency of about 35 cycles per second with decreasing amplitude as the test vehicle decelerates. Coincident with the opening process, the riser attains full line stretch and begins to oscillate in a "rope-skipping" motion that damps as the breathing subsides.

A motion-picture supplement has been prepared and is available on loan. A request card form and a description of the film will be found at the back of this paper, on the page immediately preceding the abstract page.

Overinflation characteristics.- The overinflation phenomena are associated with high aerodynamic forces acting on the canopy ribbons at supersonic speeds. The exact nature of the flow through the canopy is uncertain; however, the study presented in reference 4 and the data of reference 1 indicate the occurrence of choking with complicated shock patterns on the canopy at supersonic speeds.

The overinflation apparently arises from the mechanical adjustment of the elastic load-supporting ribbons to the stagnation pressures behind the canopy shocks. Since the ribbons are elastic, the pressure distribution across each ribbon face changes as the ribbons deform, or camber, thereby causing the porosity and the mass flow through the canopy to vary. The resilience of the material tends to restore the ribbons to their original shape, thus setting up the conditions for another loading cycle. As the test vehicle decelerates, the canopy shocks decrease in intensity and change in character.

Several canopies sustained damage due to high stagnation pressures during the tests at the highest Mach numbers. Individual horizontal and vertical ribbons were torn in the conical portion of the canopy. In addition, vent-band and radial-ribbon fraying were noted. It is believed that the ribbon failures occurred at the time of the opening shock, or shortly thereafter. There is no evidence that these failures adversely affected the parachute performance. Since the drag-producing surfaces are comprised of elastic load-supporting ribbons, the tensile loading normally carried by the failed ribbon is absorbed by adjacent ribbons. These tensile loads are transferred to the very heavy radial ribbons, carried to the skirt band, and then to the shroud lines. The theory advanced in reference 5 shows that tensile loads are highest in the horizontal ribbons in the conical portion of a fully inflated, shaped canopy.

The test data indicate that there is a Mach number boundary where the canopy breathing with overinflation decreases to essentially zero amplitude. Figure 5 presents a plot of the lower Mach number boundary ($M = 1.14$) at which the canopy oscillating load ceased in the range of dynamic pressures covered in these tests. The upper boundary in the figure represents the Mach number at which choking theoretically takes place with a detached normal shock in a stream tube having an area ratio equivalent to the canopy porosity of 28 percent (ref. 6).

Canopy stability.- The parachute stability was qualitatively evaluated by comparing the high-speed movies from the tests of the two basic canopy designs. Generally, the flat-design canopies exhibited one or two squidding motions during the initial inflation, followed by violent breathing, random coning oscillations, and a rotation of the canopy. The combination of canopy breathing and rotation caused an abrasive action between the shroud lines which resulted in the loss of the canopy on the first test. Shortening the riser by 10 feet had no apparent effect on canopy stability. These instabilities were not reduced to an acceptable level until the shaped conical canopy with a low-elongation riser was finally evolved in the test series. This canopy made possible the investigation of the parachutes at supersonic speeds.

Drag Characteristics

Canopy-riser forces.- Figures 6(a) to 6(e) present force time histories taken from the tensiometer foil recordings. An inspection of the figures shows a similar pattern of abrupt transient forces.

The tensiometer recording device was started shortly after firing the mortar by a lanyard fastened to the riser near the attach point on the test vehicle. Time zero was assumed to be mortar firing, thus the elapsed time before a significant force appears is the time required to pay out the riser. Differences in this time interval are due mainly to timing inaccuracies of the recorder and small differences in the charges of black powder used in the mortar.

The first peak in each time history of figure 6 is due to the snatch force required to accelerate the canopy mass up to the velocity of the test vehicle. Following this peak, the riser force slackens momentarily until the canopy begins to inflate. The first stage of the inflation is distinguished by a second, and generally higher, peak resulting from the opening shock. Studies of the high-speed movies show that the opening shock occurred at an inflated diameter somewhat smaller than the steady-state diameter. Following the opening shock is another brief interval of relaxation believed to be due primarily to riser elongation. A secondary cause, however, may be the nominal decrease in diameter following the opening shock, as shown in the photographic records.

The final stage of canopy inflation in figure 6 is typically represented by the series of increasing, but small, sawtooth peaks caused by a continuous diametral increase with unsymmetrical, partial collapses of one or two of the gores. The point where the force finally levels off is the instant at which the canopy is considered to be fully inflated and produces maximum inflated drag. At this time the rapid breathing motion of the canopy and the periodic overinflation began, as pointed out previously. The frequency of breathing varied from 32 to 38 cycles per second within the oscillatory-load envelopes shown in the figures. The oscillating-load envelope shown in figure 6(a) for a subsonic Mach number is believed to result from a low-amplitude breathing oscillation without the attendant overinflation noted at supersonic speeds. The assessment of the data for this particular test was hampered by the malfunctioning of the test-vehicle movie cameras. However, the magnitude of the oscillating force and the low data point appearing in figure 5 indicate that this test Mach number is below the boundary at which overinflation occurs, although canopy breathing may still take place.

Figure 6 shows that the maximum drag force was attained at full inflation, then decreased rapidly to a steady-state condition as the

oscillating forces damped out. From time 1.0 to 20 seconds, the test vehicle normally dropped 5,000 feet, decelerated to subsonic speed, and underwent a change in flight-path angle from 0° at launch to about -45°. The drag during this time diminished to a minimum level and began a gradual increase until equilibrium was attained. The internal records and trajectory analysis show that equilibrium drag (retarding force equal to suspended weight) was normally reached about 40 seconds after release. The flight path was essentially vertical, and the rate of descent depended solely on air density. Generally, the test vehicles impacted 3 minutes after launch.

A review of the time histories (fig. 6) shows that the snatch force is relatively minor in the sequence of abrupt transient forces. The opening-shock forces, on the other hand, are relatively high and exhibit a slight decrease with increasing Mach number, but a significant increase with increasing dynamic pressure (figs. 6(c) and 6(d)). The drag of the inflated canopy increases with Mach number and dynamic pressure and eventually exceeds the opening shock.

Opening-shock drag coefficient.- Opening-shock drag coefficients are shown in figure 7 as a function of Mach number. Data from sled tests at subsonic speeds for similar ribbon parachutes (ref. 7) are included for comparison with the free-fall test data. Values of opening-shock drag coefficient calculated by using the method presented in reference 8 are also shown. Reference 8 clearly states that the method for calculating opening shock does not take into account compressibility effects and that the calculations, therefore, are not valid above $M = 0.90$. The theoretical value is constant with Mach number since the drag, according to this method, is essentially a linear function of dynamic pressure.

The data from the present tests show a decrease in opening-shock drag coefficient as Mach number is increased from about 1.0 to 1.5. Comparison of these data with data from the subsonic sled tests indicates the existence of a typical transonic drag rise. The opening-shock factor (ratio of opening-shock force to inflated drag force) is presented in figure 8 as a variation with Mach number. These data show that the opening shock is approximately 40 percent greater than the inflated drag near $M = 1.0$, decreasing to about 60 percent of the inflated drag near $M = 1.5$.

It is of interest to compare the limited flat-canopy data of the present tests in figures 7 and 8 with respect to the effect of canopy porosity. Figure 8 shows that the opening-shock factors are approximately equivalent; therefore, the inflated drag forces are compatible with the respective opening shocks. In figure 7 the opening-shock drag coefficient for the high-porosity canopy is substantially lower than that of the low-porosity canopy, indicating that porosity affects

the opening-shock magnitude. The data from the shaped conical canopy fall between the extremes of the flat-canopy data.

It appears, then, that the opening shock is affected not only by Mach number but also by the porosity, the location and intensity of shocks on the canopy, and the individual ribbon loading and elasticity. Porosity also affects the canopy filling time and, thus, the rate of energy absorption, or stopping power, of the canopy. It is also believed that shroud-line elasticity may absorb some part of the opening shock as the opening shock becomes greater.

Inflated drag coefficient.- The inflated drag coefficient is presented in figure 9 as a variation with Mach number. This coefficient is based on the maximum inflated drag force (mean value, figs. 6(d) and 6(e)) occurring at the time of initial canopy inflation following the opening shock. Although canopy-inflation instabilities are apparent, this time is chosen for defining inflated drag because the Mach number is essentially unchanged from that at canopy deployment. This point also is representative of the maximum drag force experienced during each deployment. The drag of the inflated canopy rapidly decelerates the test vehicle, and the Mach number changes significantly within 2 to 3 seconds after inflation.

In figure 9 the gradually increasing inflated drag coefficient indicates that the canopy is experiencing compressibility effects with increasing Mach number. The inflated drag coefficient is also interrelated with the aerodynamic forces which produce canopy breathing. The inflated drag force increases more rapidly with Mach number than with dynamic pressure, thereby resulting in an increasing drag coefficient.

The flat-canopy data (fig. 9) of the present tests, obtained in the low supersonic region, show the effect of porosity on the magnitude of the inflated drag coefficient. Near sonic speed, the inflated drag coefficient of the 30-percent-porosity canopy is approximately two-thirds that of the shaped conical canopy and of the flat canopies with relatively low porosities.

Figure 10 is a summary plot of drag-coefficient variations with Mach number, comparing the performances of high- and low-porosity flat canopies with the high-porosity, shaped conical canopies. The data are presented in the form of time histories from deployment at high Mach numbers to essentially stabilized conditions in vertical descent at the lowest Mach numbers. It can be seen from the data shown in figure 10(a) that an increase in the porosity of the flat canopy from 17.5 percent to 30 percent reduces the measured drag coefficient by a factor of approximately one-third over the Mach number range.

Comparing the data of figure 10(b) with 10(a) shows that the shaped-conical-canopy design, with a relatively high constructed porosity, produces a drag equivalent to that of a flat-canopy design with relatively low porosity.

Comparison of Measured and Calculated Forces

Opening shock and snatch force were calculated for the Mach number and altitude conditions at parachute deployment by using the method suggested in reference 8. The method was applied directly without corrections for compressibility above $M = 0.90$. The results of the calculations are compared with experimental results in figure 11.

Snatch force.- The snatch-force calculations are based on the elastic characteristics of the riser and the mass of the canopy. Material properties were taken from limited empirical data for a riser material similar to that used in the present program. The calculated results, in general, appear to overpredict the measured values. The differences are believed to be related to the mechanics of the deployment process which have a significant effect on the measured snatch forces. For example, the technique of tying the riser into the deployment bag with light break cord causes a series of small forces to act on the packed parachute, thus reducing the total inertia to be overcome when the riser is fully extended. Forcible deployment of the low-drag packed canopy is desirable from the standpoint of insuring canopy extraction from the bag. However, this method increases the relative separation velocity, thereby imparting additional momentum to the canopy mass and, in turn, increasing the snatch force.

Opening shock.- Opening-shock calculations are based on mass-flow characteristics through the porous ribbon canopy, with flow coefficients and filling time as parameters. Assuming constant flow coefficients and a very short filling time, the opening-shock equation becomes a linear function of dynamic pressure.

The calculations indicate that theory again overpredicts the measured forces at the higher force levels associated with high dynamic pressures and Mach numbers. At the lower dynamic pressures and Mach numbers, however, the theory tends to underpredict the measured values. These discrepancies are believed to be caused by the failure of the theory to account for Mach number effects and mass-flow discontinuities due to shocks on the canopy. In addition, the extremely rapid inflation time of the relatively small canopies introduces other effects not considered for the theory of reference 8.

CONCLUSIONS

The results of a development program to provide a suitable drogue-stabilization parachute for the Project Mercury capsule lead to the following conclusions:

1. An acceptable parachute was developed for use as a first-stage drogue-stabilization device.

2. A high-porosity, shaped conical-ribbon canopy was a more efficient and stable drag-producing device than a flat-ribbon canopy with equivalent porosity.

3. Mach number and constructed porosity were major parameters which governed the opening-shock and inflated drag-coefficient characteristics of the test parachutes.

4. High-frequency canopy breathing with overinflation occurred at Mach numbers greater than 1.14 as a result of fluctuating critical pressure ratios associated with shock waves existing on the inflated canopy.

5. High stagnation pressures associated with shock waves were believed to cause failures of highly loaded ribbons in the conical portion of the inflating canopy.

6. The ribbon-canopy opening-shock factor showed that the opening shock was 40 percent greater than the inflated drag force near a Mach number of 1.0, but decreased to about 60 percent of the inflated drag near a Mach number of 1.5.

Flight Research Center,
National Aeronautics and Space Administration,
Edwards, Calif., July 29, 1960.

REFERENCES

1. Connors, James F., and Lovell, J. Calvin: Some Observations on Supersonic Stabilization and Deceleration Devices. Paper No. 60-19, Inst. Aero. Sci., Jan. 1960.

2. Anon.: United States Air Force Parachute Handbook. WADC Tech. Rep. 55-265, ASTIA Doc. No. AD 118036, Wright Air Dev. Center, U.S. Air Force, Dec. 1956.

3. Schulze, Curt D.: Accuracy Investigation of Coleman Mechanical Tensiometer. AFFTC Tech. Rep. 59-7, ASTIA Doc. No. AD 214627, Aug. 1959.

4. Wiant, Harry W., and Fredette, Raymond O.: A Study of High Drag Configurations as First Stage Decelerators. WADC Tech. Note 56-320, Cook Res. Lab., July 1956.

5. Jaeger, J. A., Culver, J. H., and Della-Vedowa, R. P.: A Study of the Load Distribution in a Conical Ribbon Type Parachute. Rep. No. 8541, Lockheed Aircraft Corp., Aug. 22, 1952.

6. Ames Research Staff: Equations, Tables and Charts for Compressible Flow. NACA Rep. 1135, 1953. (Supersedes NACA TN 1428.)

7. Cook Research Laboratories: Recovery Systems for Missiles and Target Aircraft. Phase 1A. AF Tech. Rep. 5853 (Contract No. AF33(038)-10653), ASTIA Doc. No. 76877, Wright Air Development Center, U.S. Air Force, Mar. 1954.

8. Wilcox, Bruce: The Calculation of Filling Time and Transient Loads for a Parachute Canopy During Deployment and Opening. Tech. Rep. SC-4151, ASTIA Doc. No. 156428, Sandia Corp., Feb. 1958.

TABLE I.- SUMMARY OF RIBBON-PARACHUTE TESTS

[Nominal 6-foot constructed diameter]

Test number	Canopy-ribbon design	Number of gores	Constructed porosity λ_g, percent	Riser material	Riser length, ft	Riser strength, lb	q_o, lb/sq ft	M_o
1	Flat	8	23	Nylon	40	9,000	67.5	1.02
2	Flat	8	17.5	Nylon	40	6,000	-----	----
3	Flat	10	30	Nylon	37.8	9,000	-----	----
4	Flat	10	30	Nylon	37.8	9,000	-----	----
5	Flat	10	30	Nylon	37.8	9,000	82.0	.93
6	Flat	8	17.5	Nylon	2	9,000	-----	----
7	Conical	8	28	Dacron	37.8	9,000	97.4	.92
8	Conical	8	28	Dacron	37.8	9,000	90.3	1.20
9	Conical	8	28	Dacron[1]	30	6,000	100.5	1.29
10	Conical	8	28	Dacron[1]	30	9,000	230.9	1.30
11	Conical	8	28	Dacron	30	9,000	91.1	1.20
12	Conical	8	28	Dacron	30	9,000	-----	----
13	Conical	8	28	Dacron[1]	30	9,000	193.3	1.52
14	Conical	8	28	Dacron[1]	30	9,000	190.0	1.48

[1]Hot-stretched.

E-4592

(a) Low-porosity (λ_g = 17.5 percent), 6-foot-diameter, flat-ribbon canopy. Painted gore for reference purposes.

Figure 1.- Photographs of test ribbon canopies.

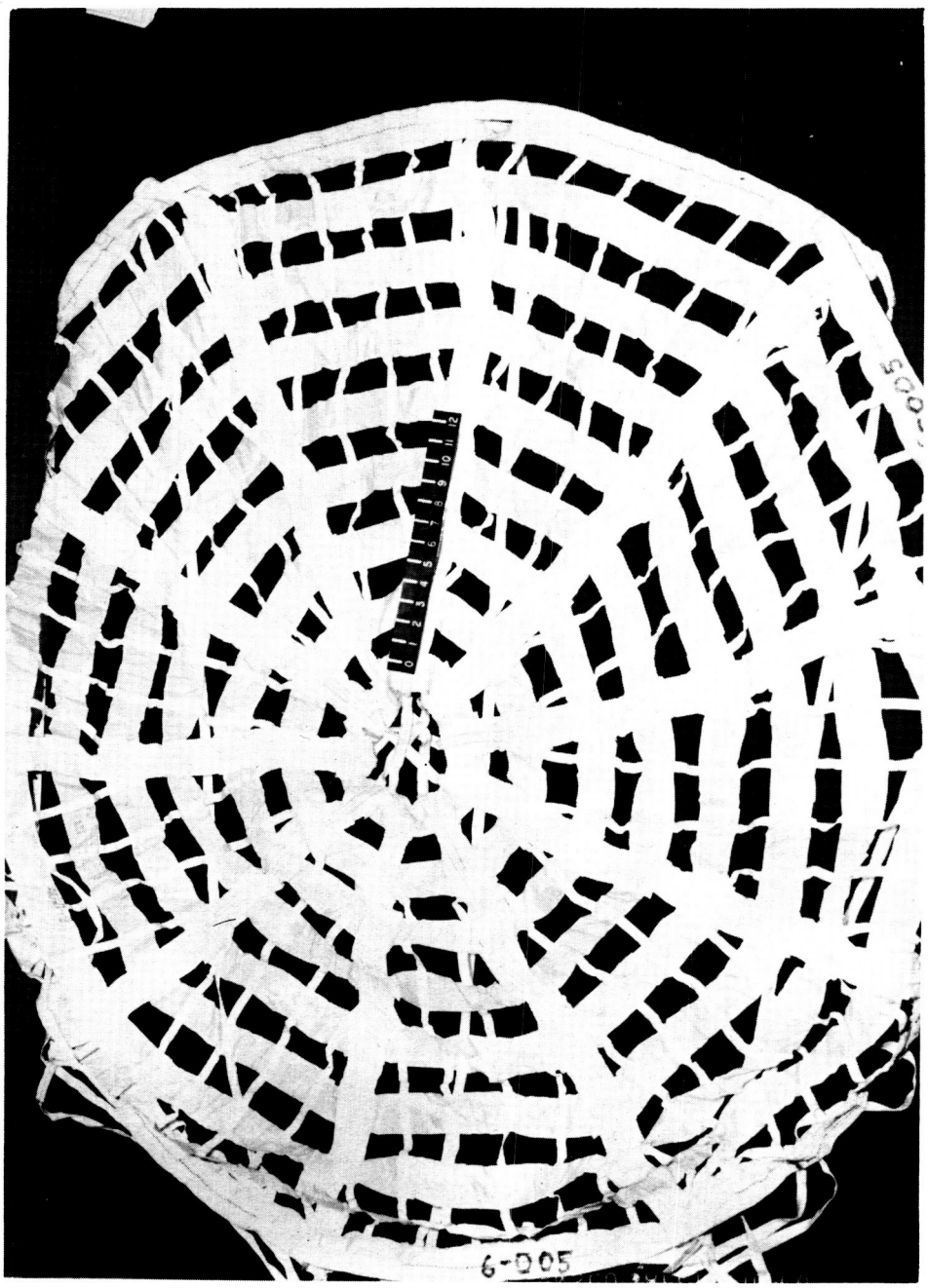

E-4631

(b) High-porosity (λ_g = 30 percent), 6-foot-diameter, flat-ribbon canopy.

Figure 1.- Concluded.

(a) Side view showing aircraft and test-vehicle configuration. E-4826

Figure 2.- Photographs of launch aircraft and mounted test vehicle.

CONFIDENTIAL

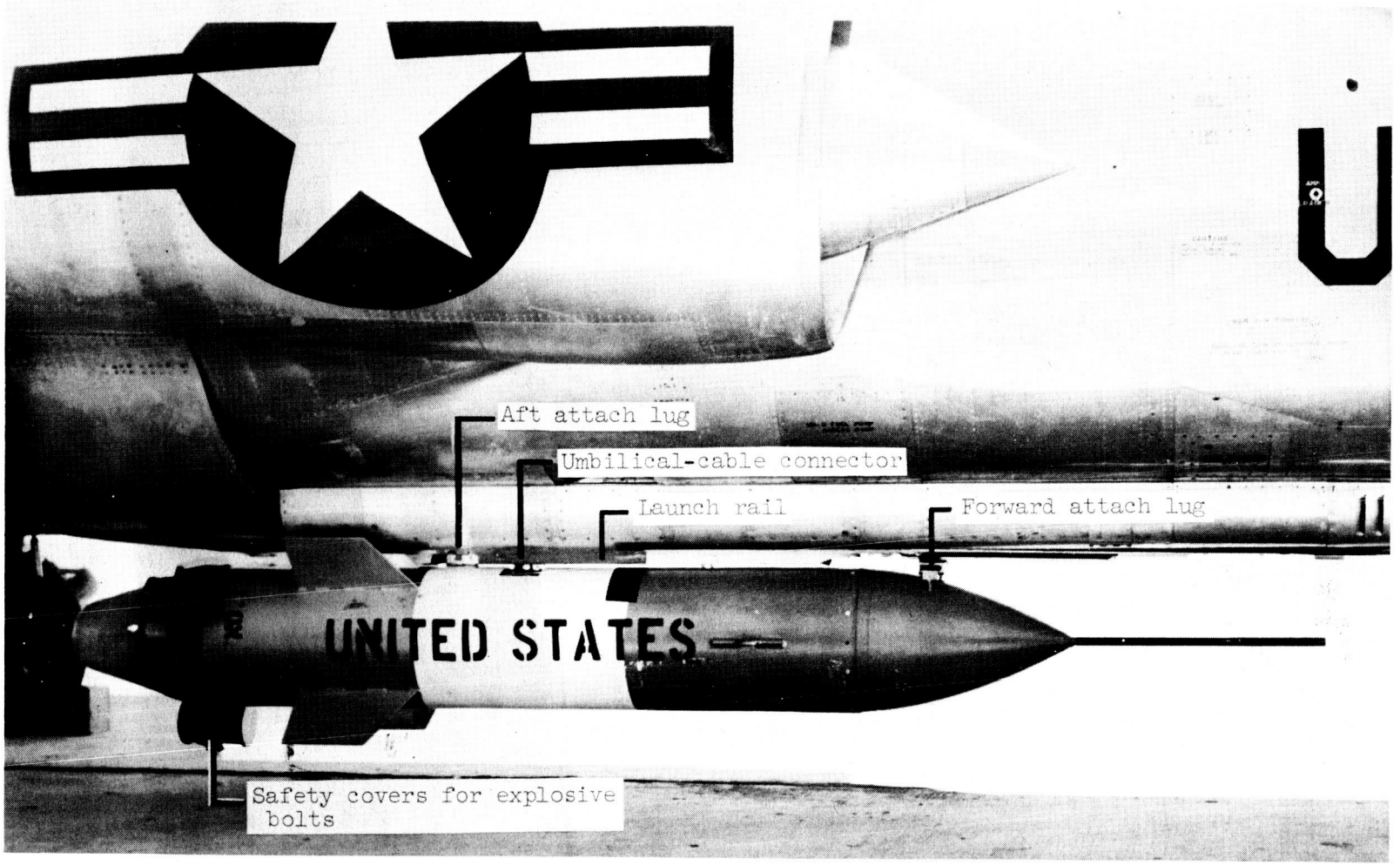

E-4580

(b) Closeup view of test vehicle showing details of attachment to launch rail.

Figure 2.- Concluded.

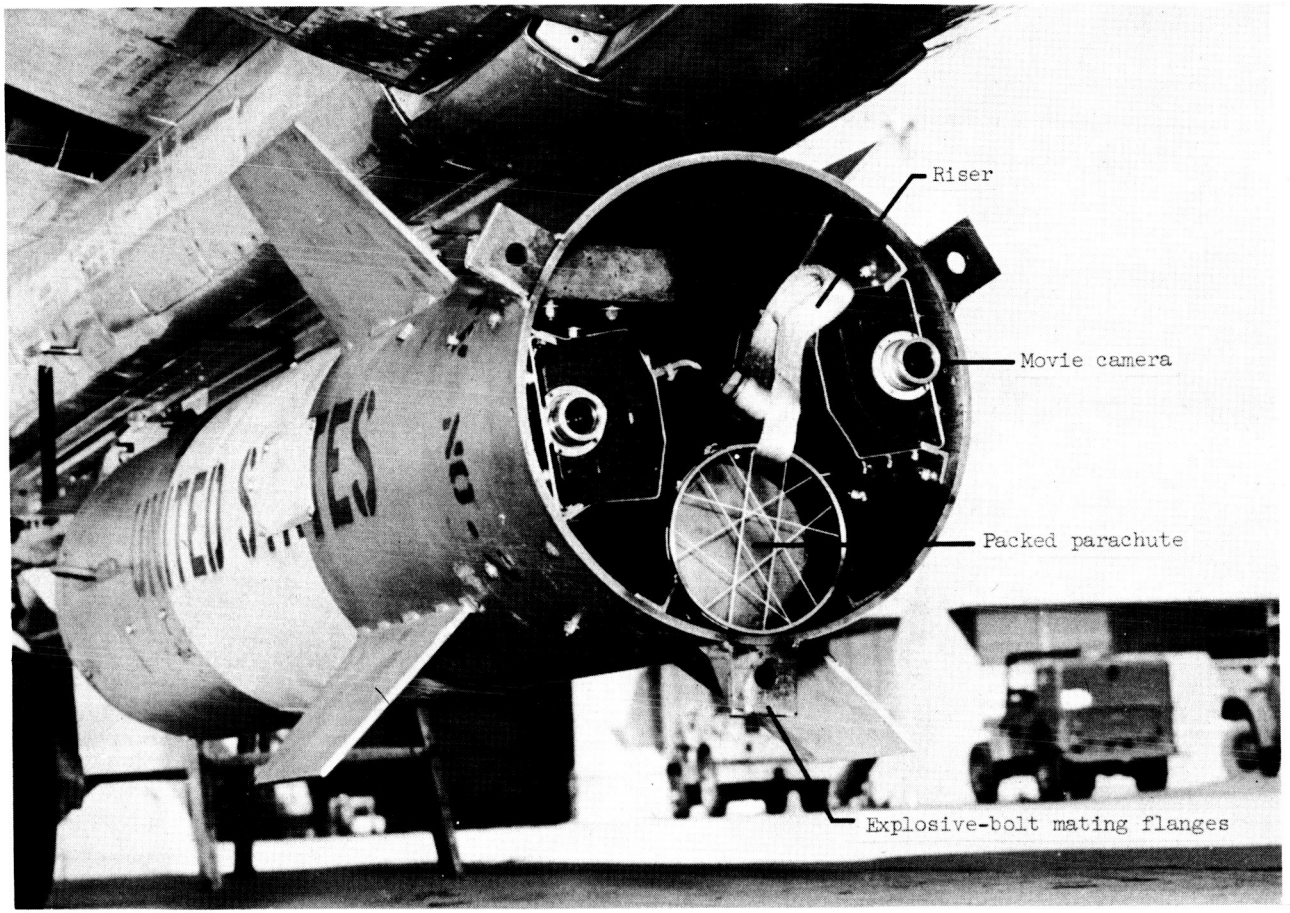

E-4635

(a) Details of noninstrumented test vehicle showing camera mounting, mortar installation, and riser-attach point.

Figure 3.- Photographs of test-vehicle instrumentation.

CONFIDENTIAL

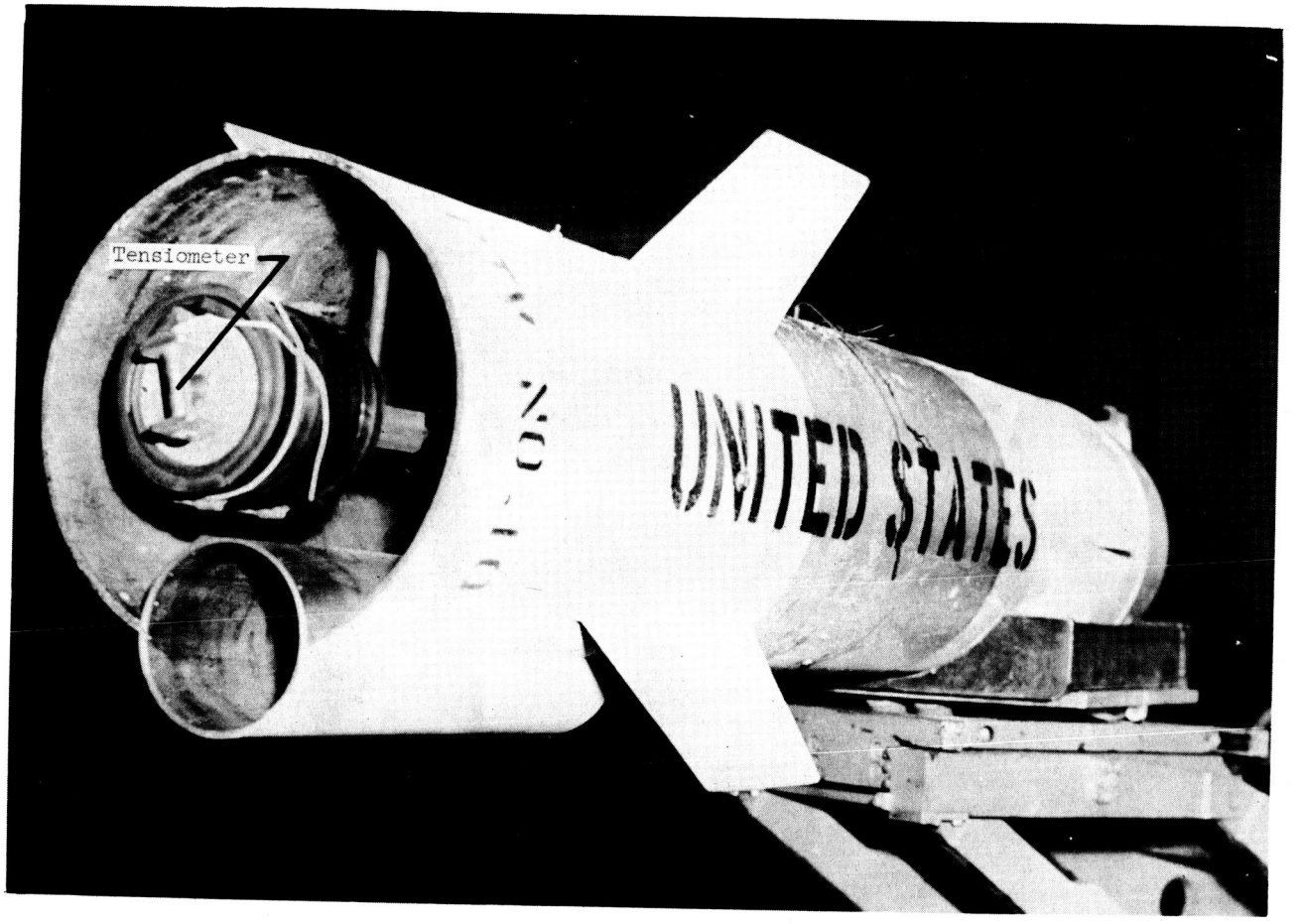

(b) Partially instrumented test vehicle showing mounted Coleman mechanical tensiometer and off-center mortar installation prior to camera installation. E-4601

Figure 3.- Continued.

CONFIDENTIAL

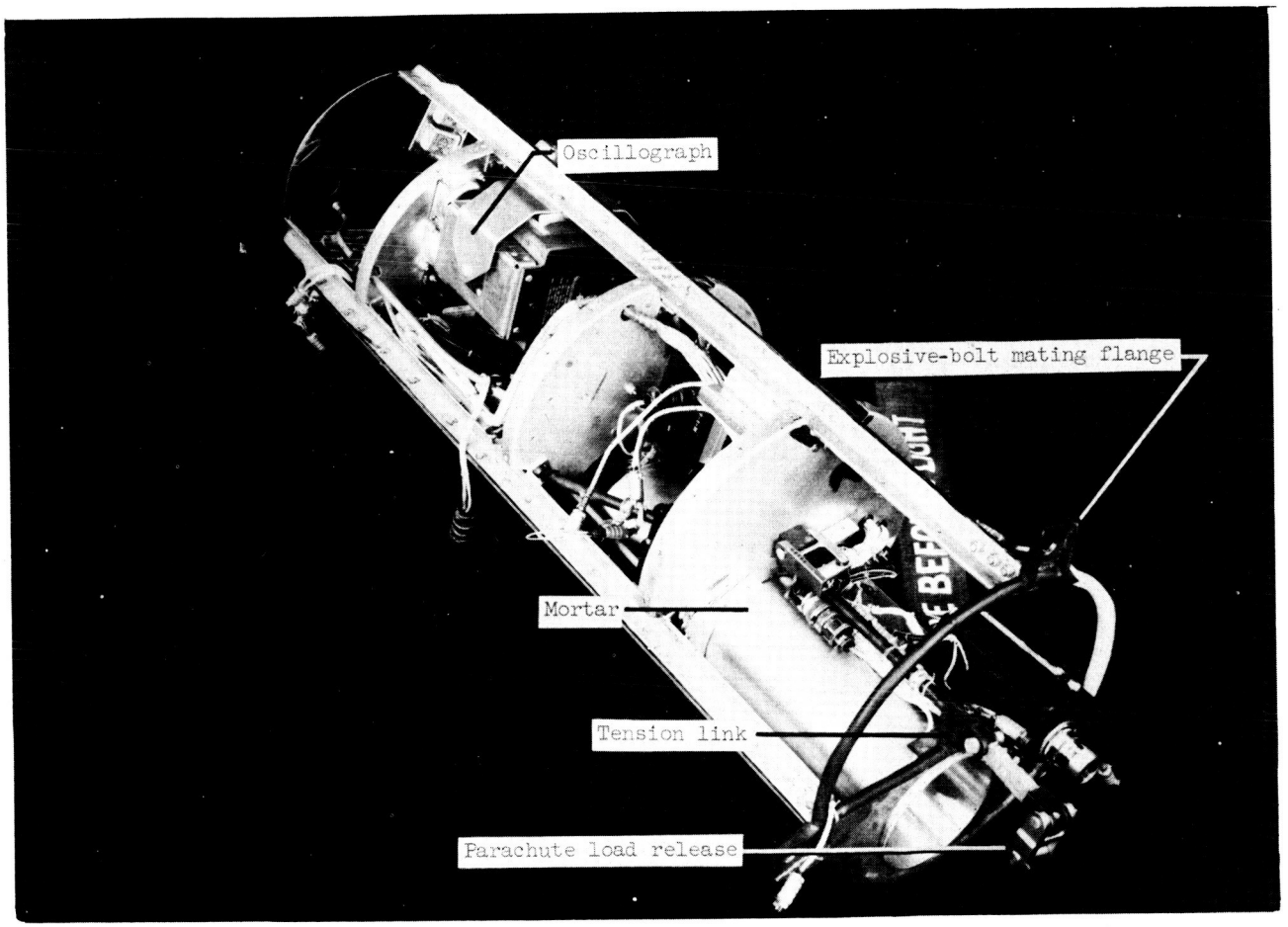

E-4731

(c) Partially assembled instrument capsule, showing test-parachute load release, tensiometer, camera, and mortar installation.

Figure 3.- Concluded.

CONFIDENTIAL

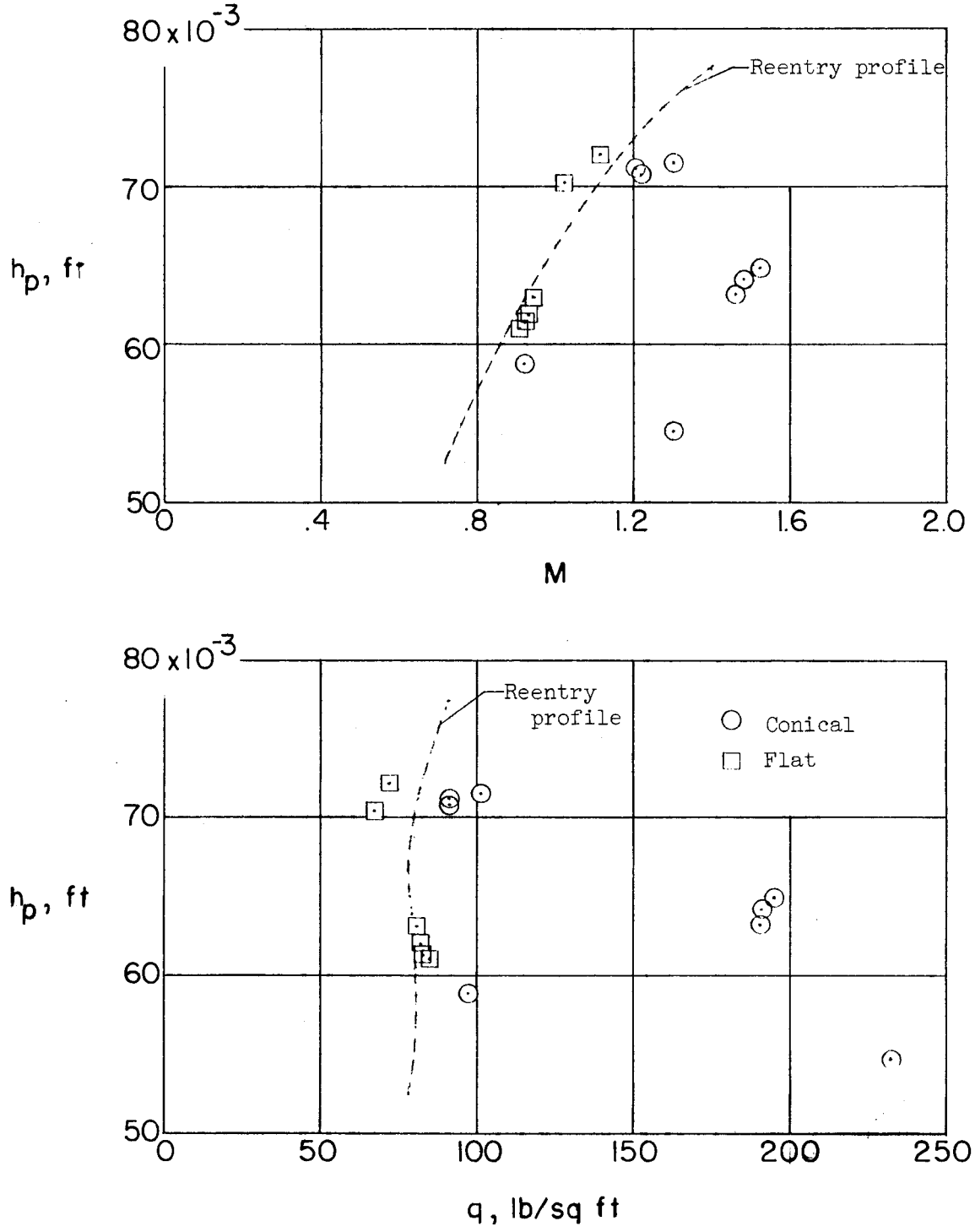

Figure 4.- Summary of test-parachute-deployment conditions and comparison with a possible Mercury capsule reentry profile.

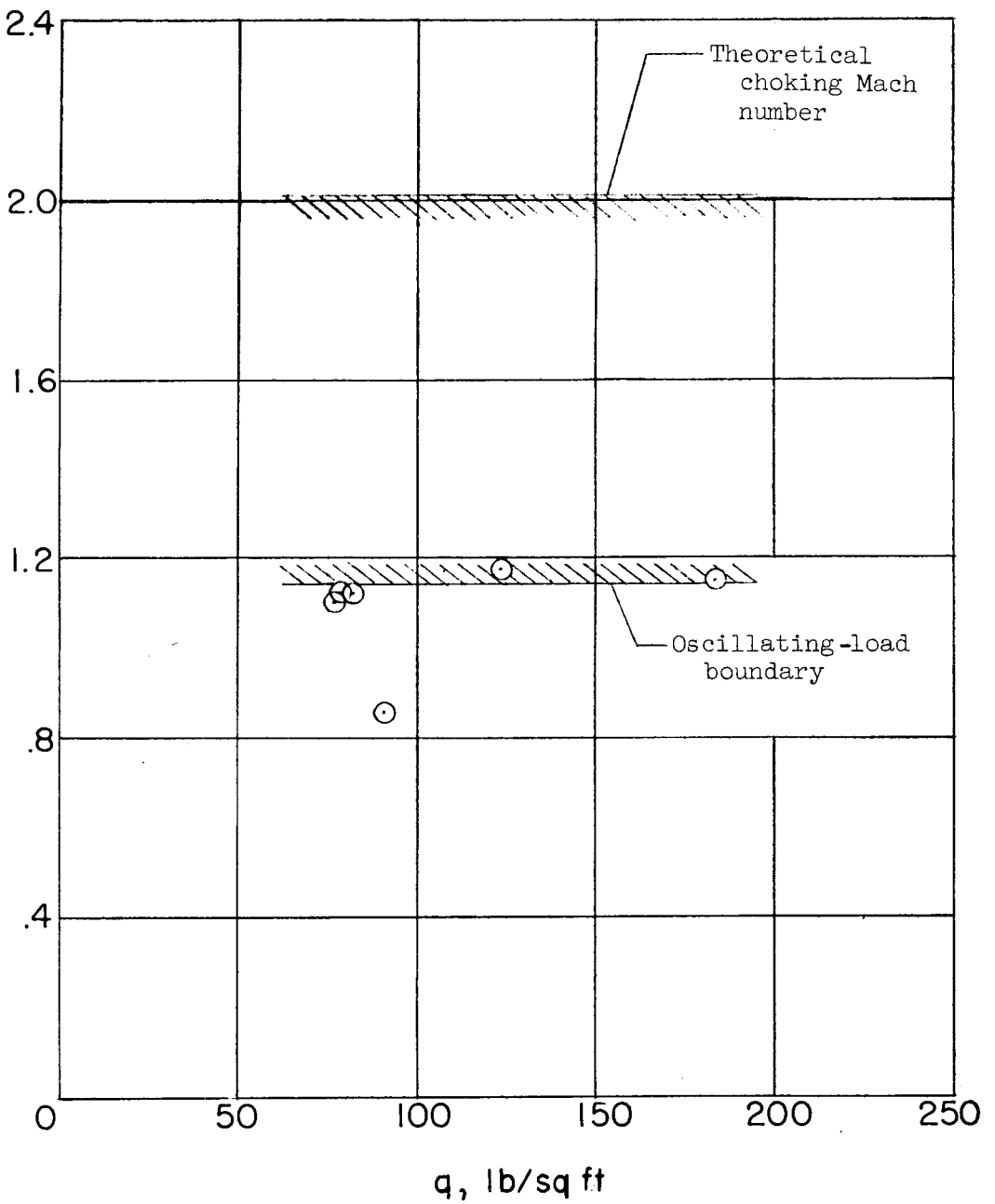

Figure 5.- Mach number plotted against dynamic pressure to show the over-inflation load characteristics as a lower-limiting Mach number boundary for a 28-percent-porosity canopy.

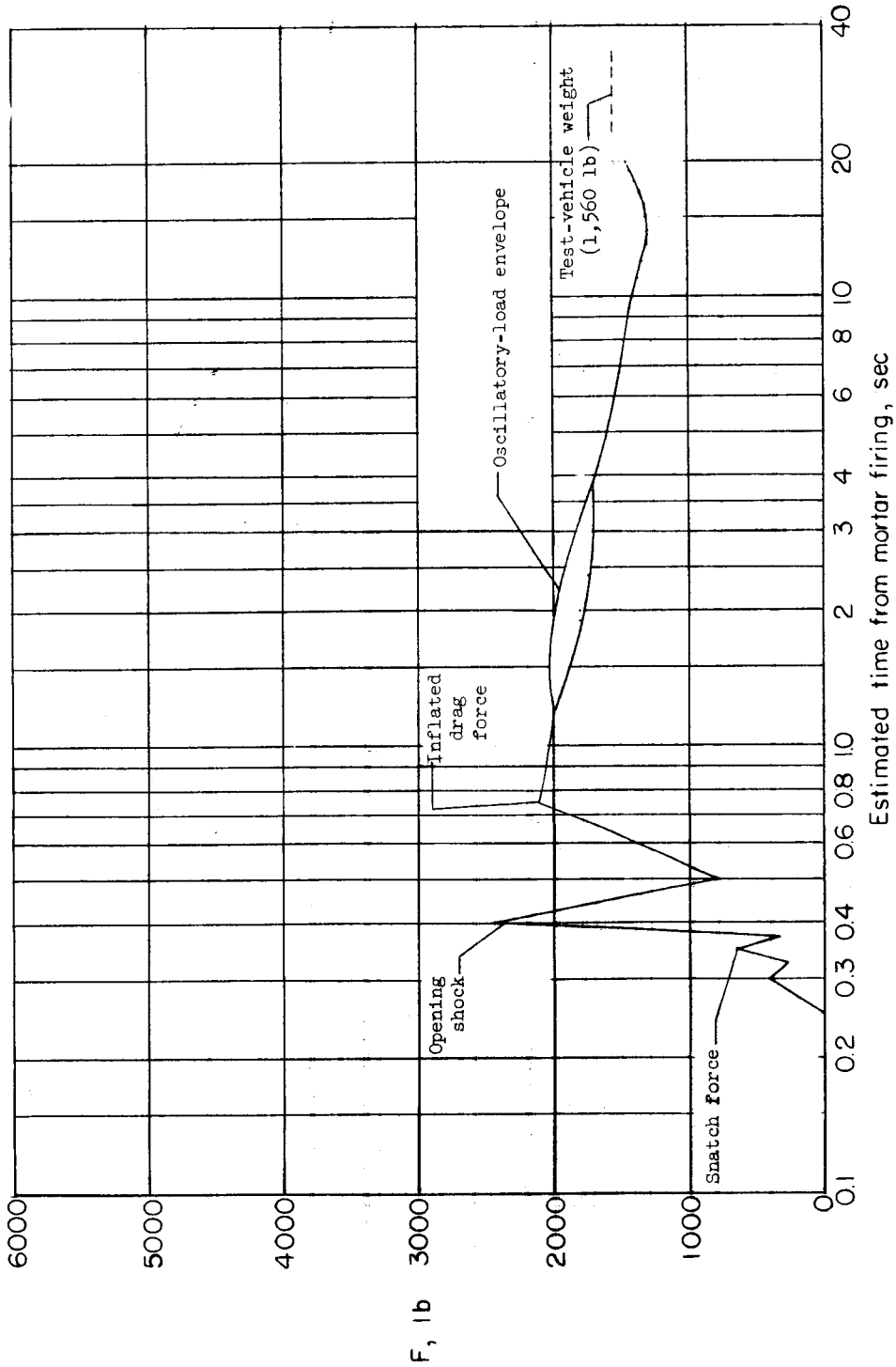

(a) M = 0.92; h_p = 58,800 ft.

Figure 6.- Tensiometer force time histories taken from tests of the conical-ribbon parachutes. Six-foot reefed diameter; λ_g = 28 percent.

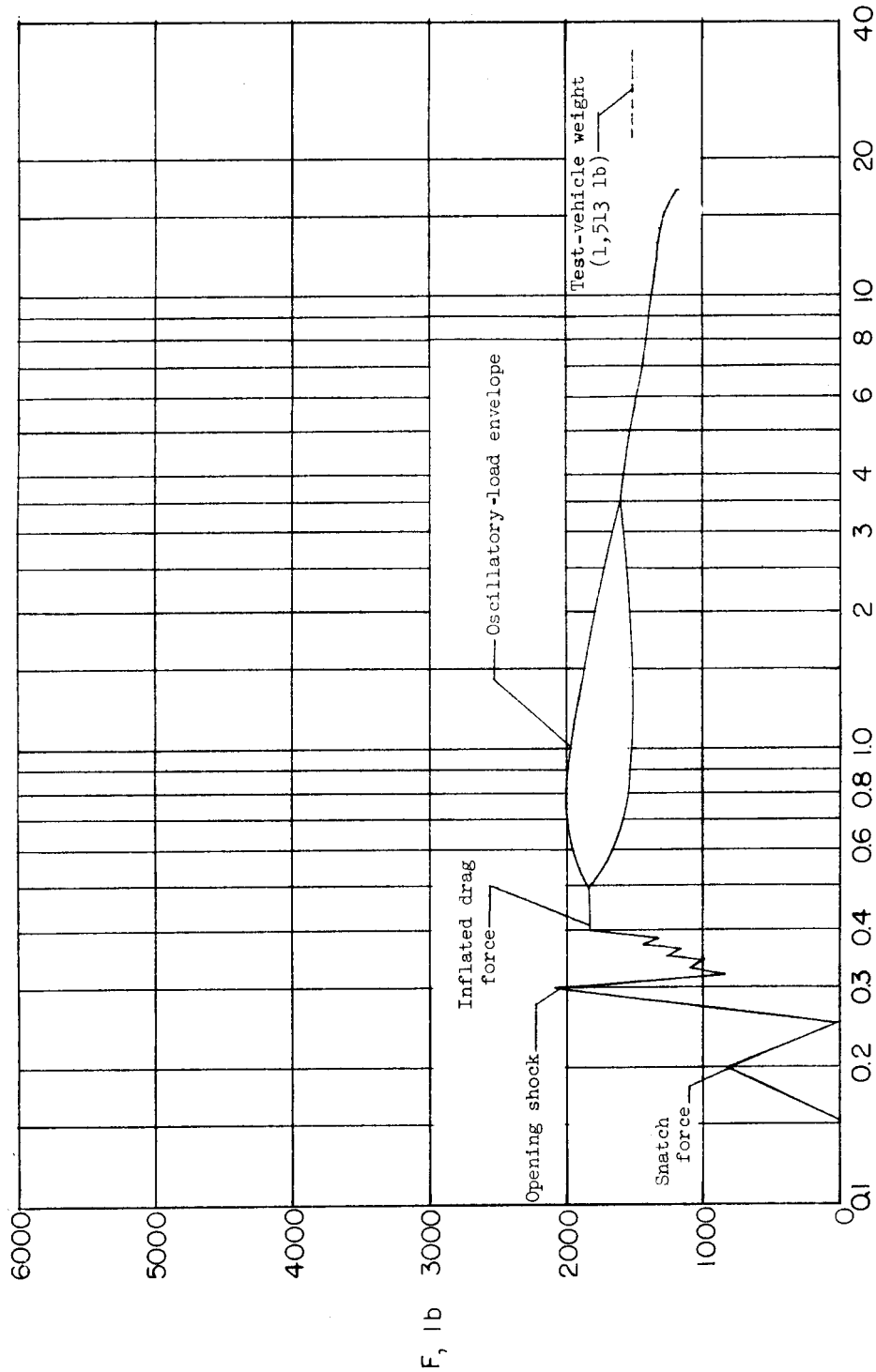

(b) $M = 1.20$; $h_p = 70,750$ ft.

Figure 6.- Continued.

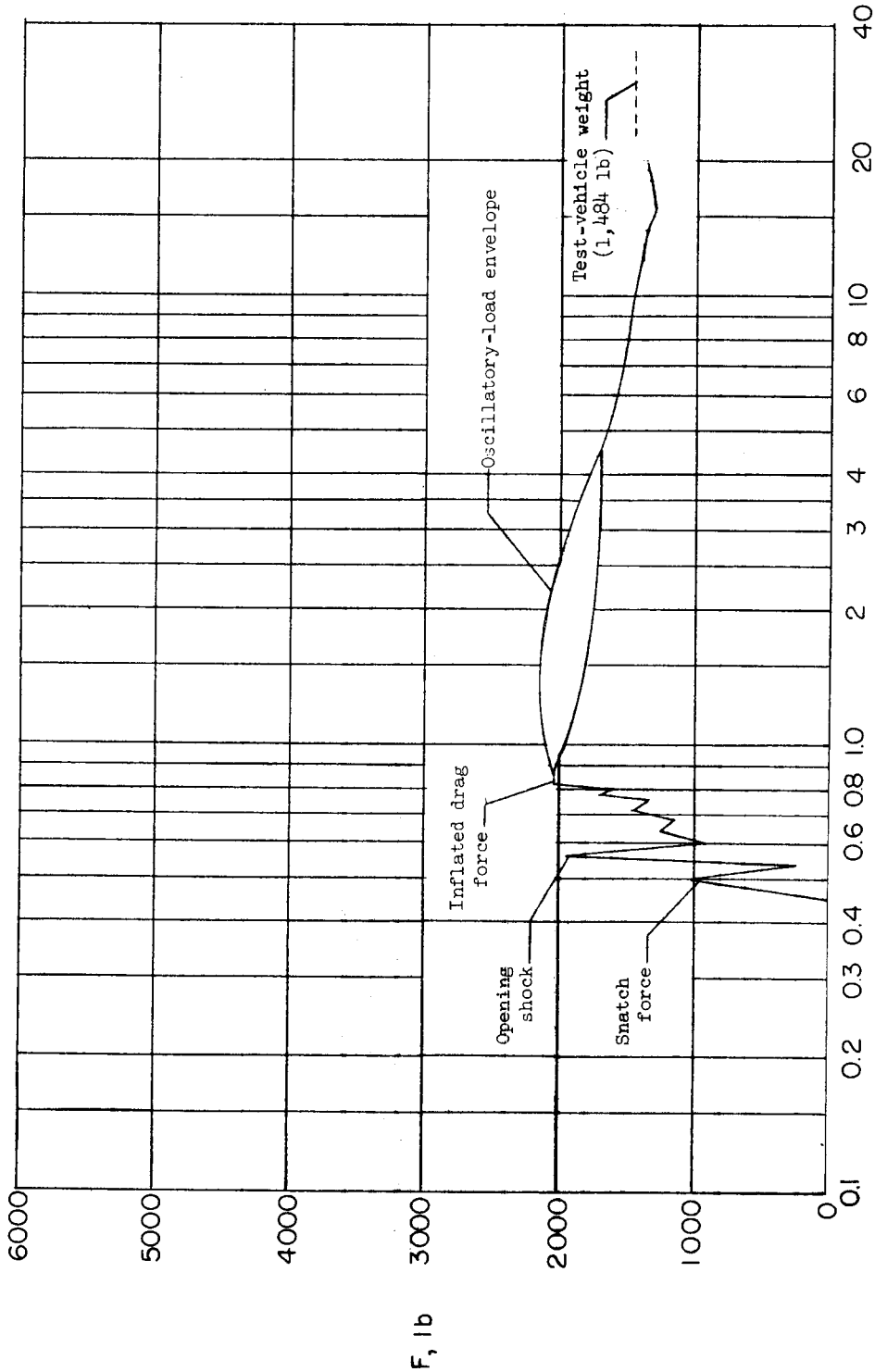

(c) M = 1.29; h_p = 71,500 ft.

Figure 6.- Continued.

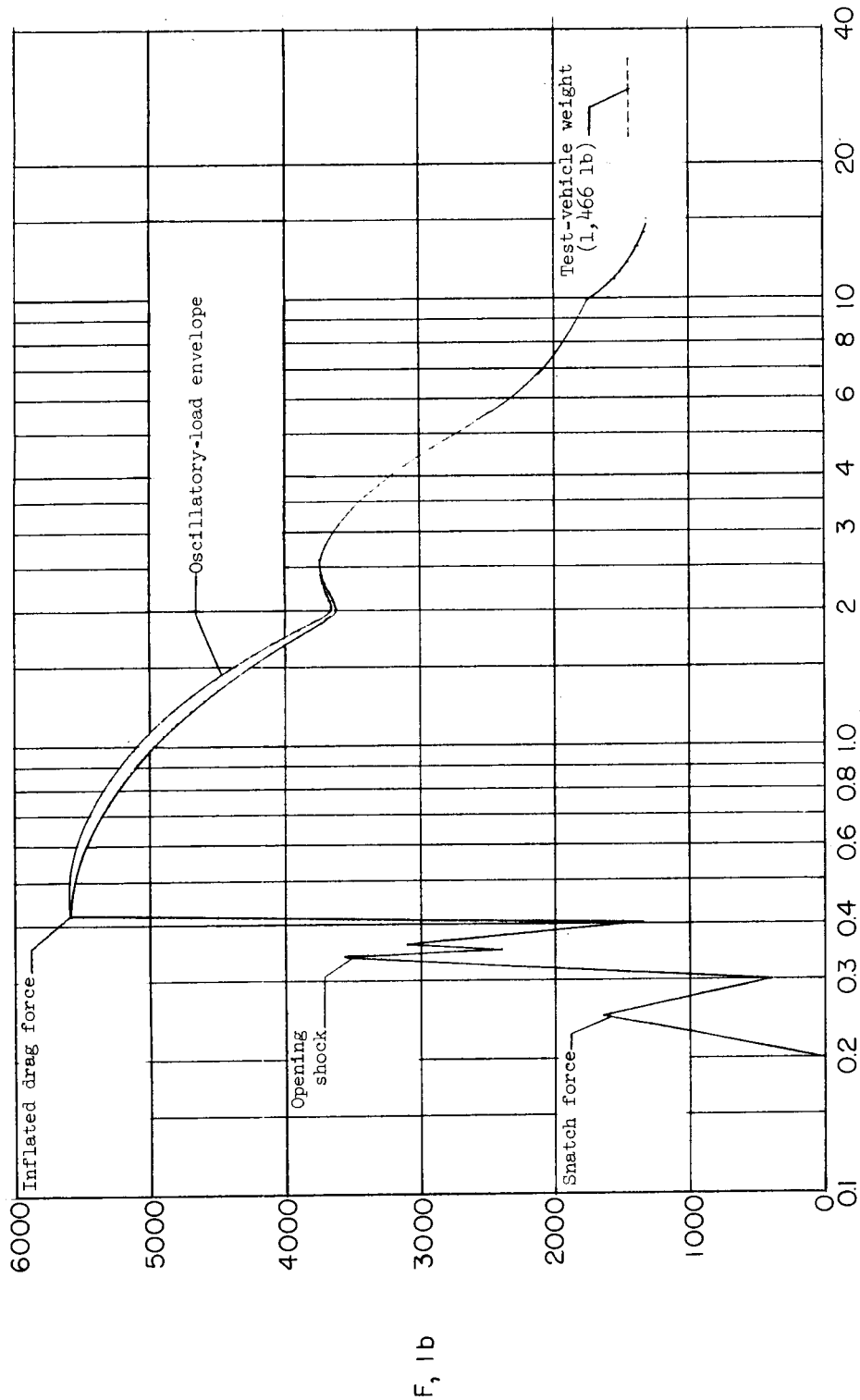

(d) M = 1.30; h_p = 54,450 ft.

Figure 6.- Continued.

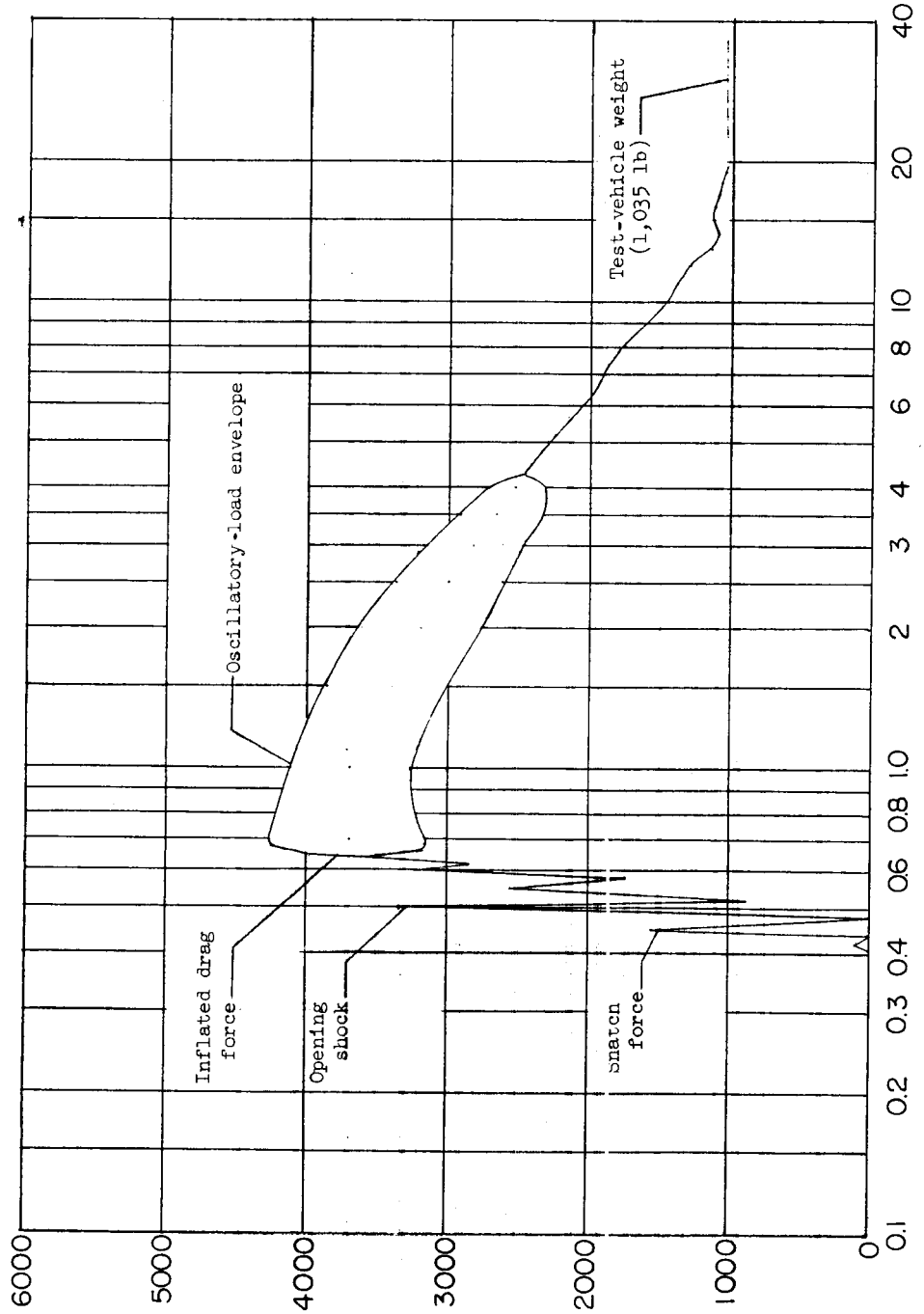

(e) M = 1.48; h_p = 64,000 ft.

Figure 6.- Concluded.

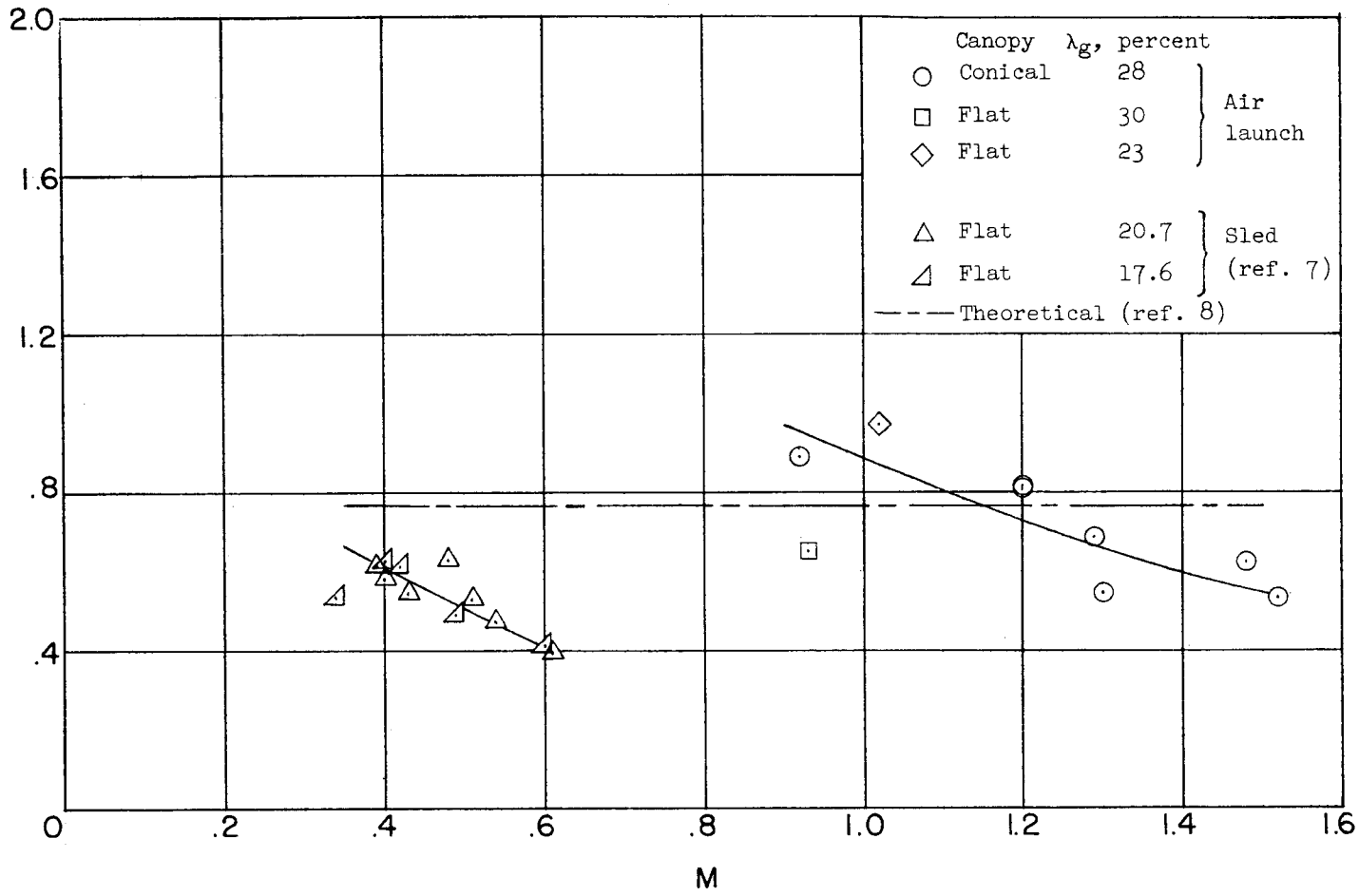

Figure 7.- Opening-shock drag-coefficient variation with Mach number showing a comparison with low-altitude subsonic sled tests.

CONFIDENTIAL

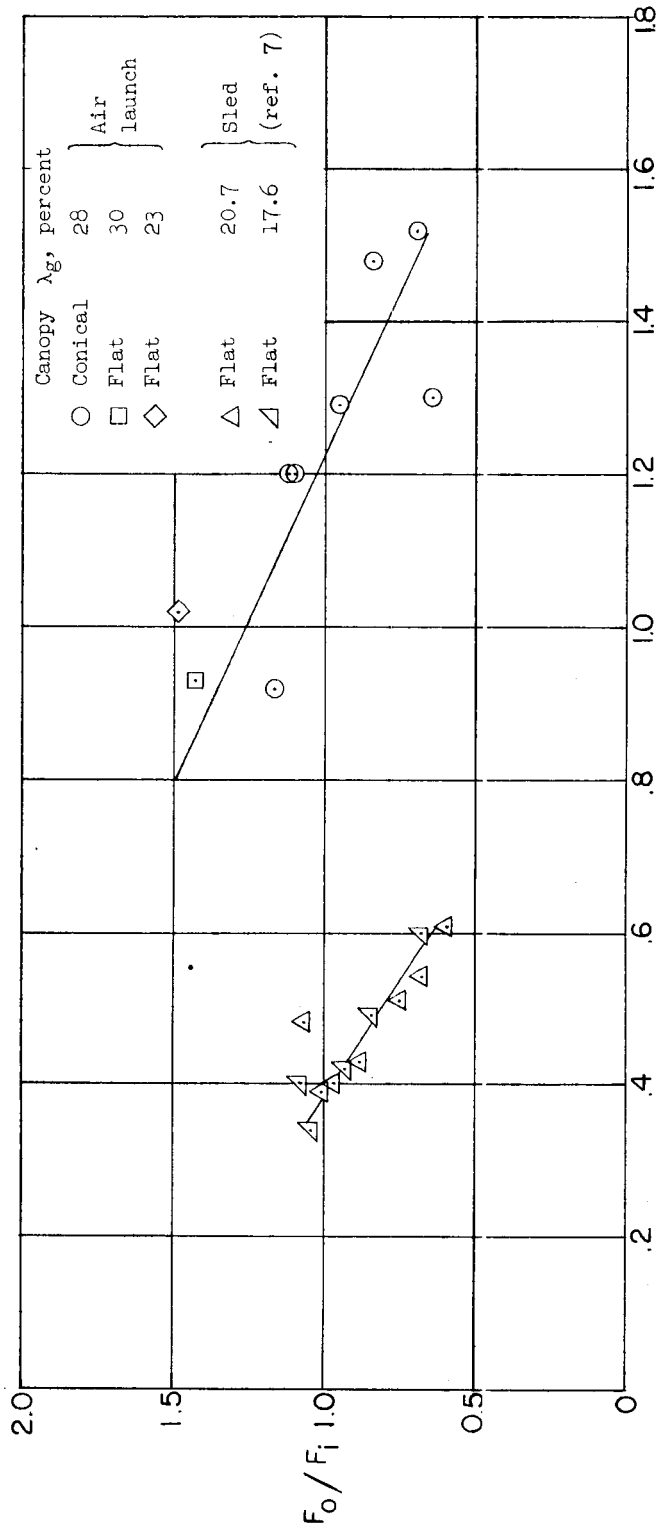

Figure 8.- Ribbon-canopy shock factor as a variation with Mach number and comparison with subsonic sled tests.

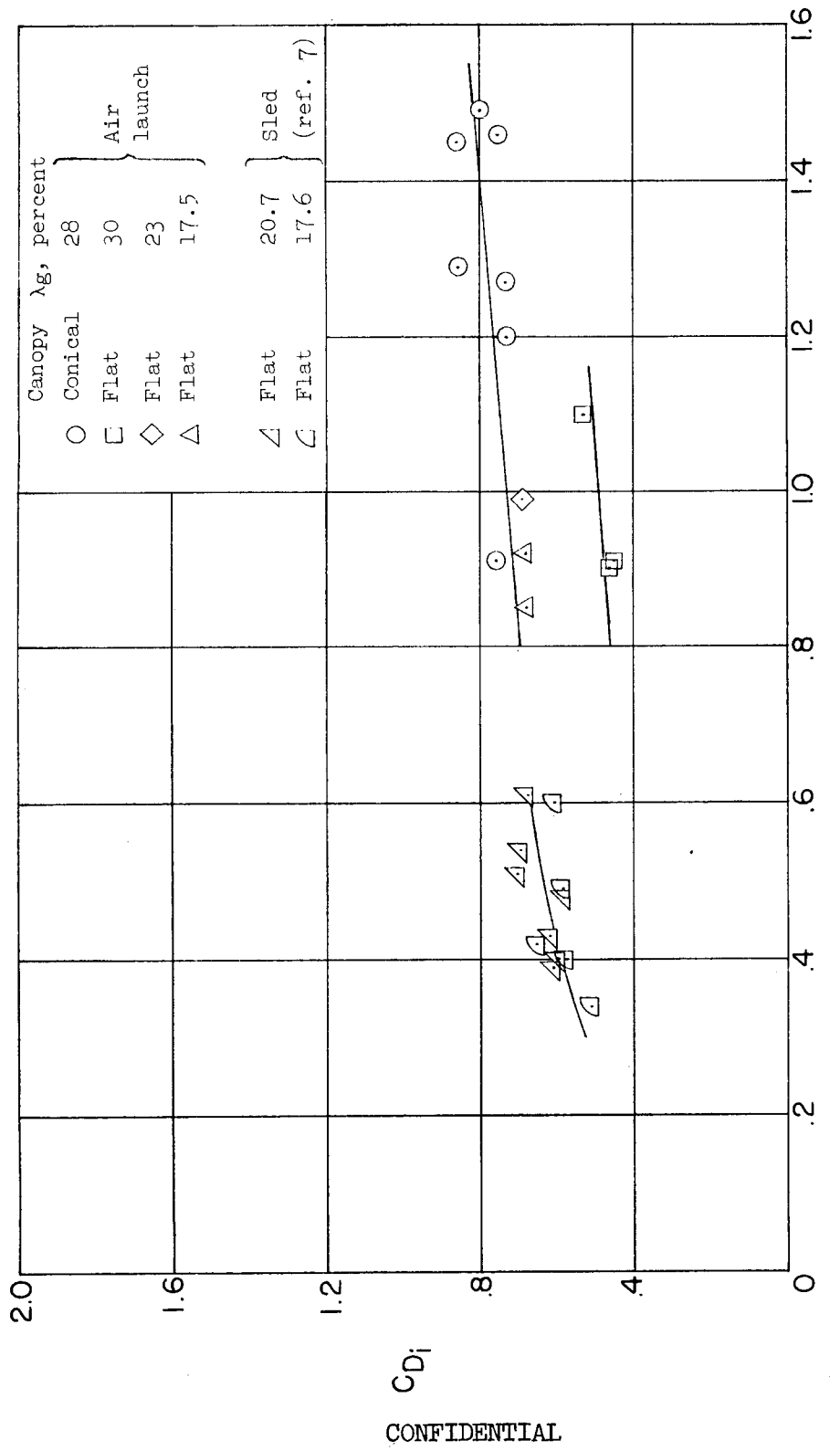

Figure 9.- Inflated drag-coefficient variation with Mach number showing porosity effects and a comparison with subsonic sled tests.

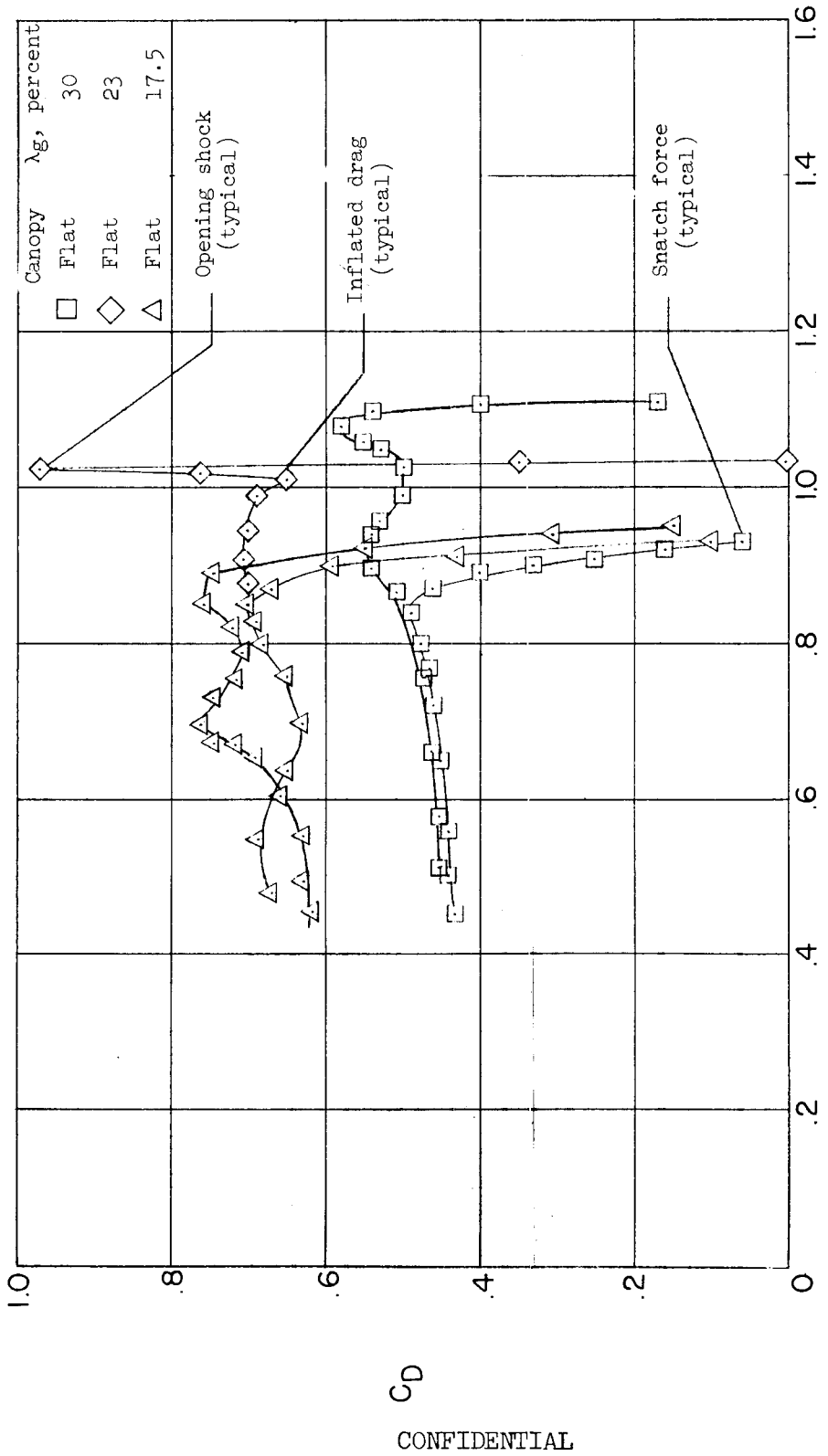

(a) Flat-ribbon-canopy performance, λ_g = 17.5 percent to 30 percent.

Figure 10.- Summary plots of drag-coefficient variations with Mach number showing porosity effects and a comparison of flat-canopy performance with conical-canopy performance.

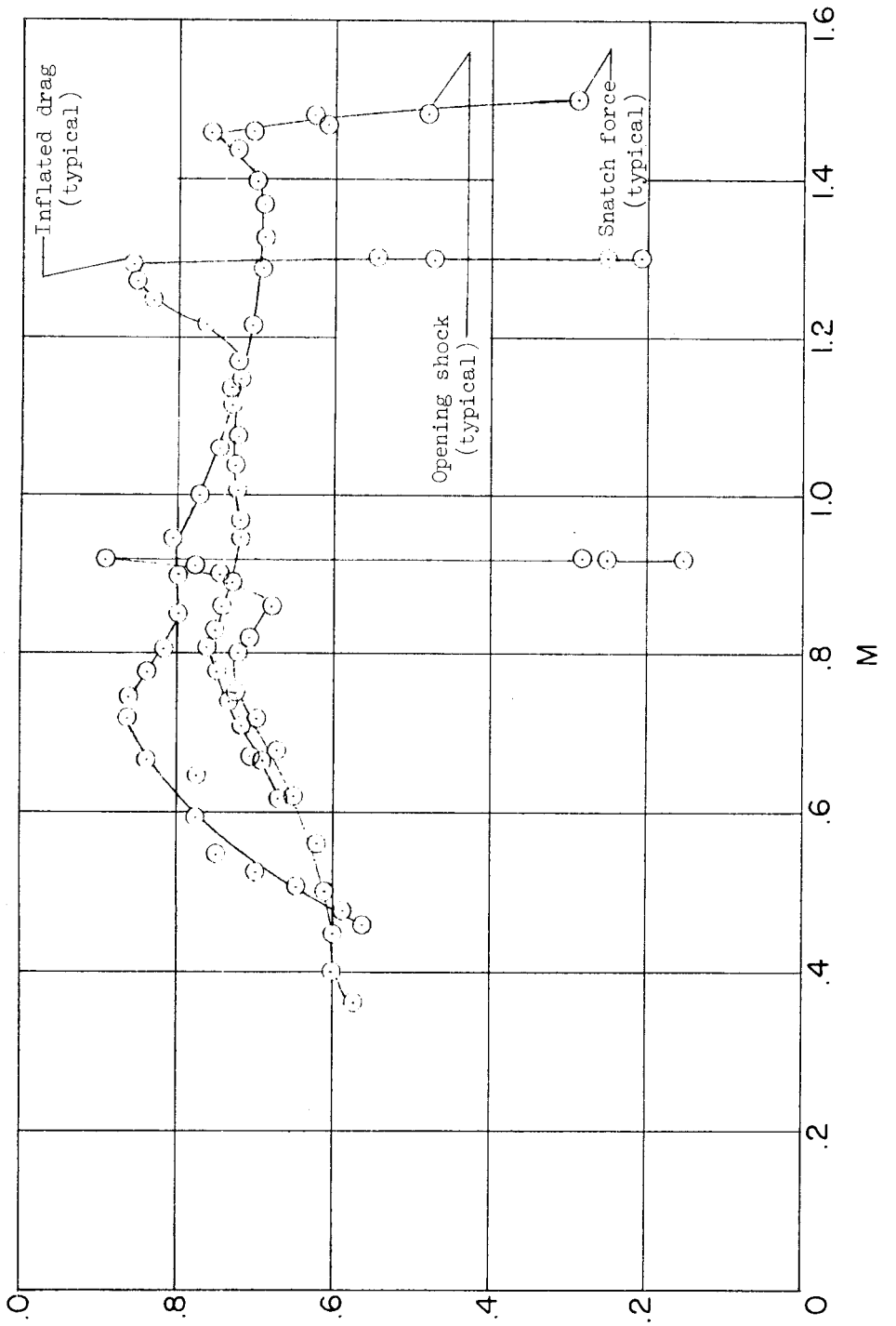

(b) Conical-ribbon-canopy performance, λ_g = 28 percent.

Figure 10.- Concluded.

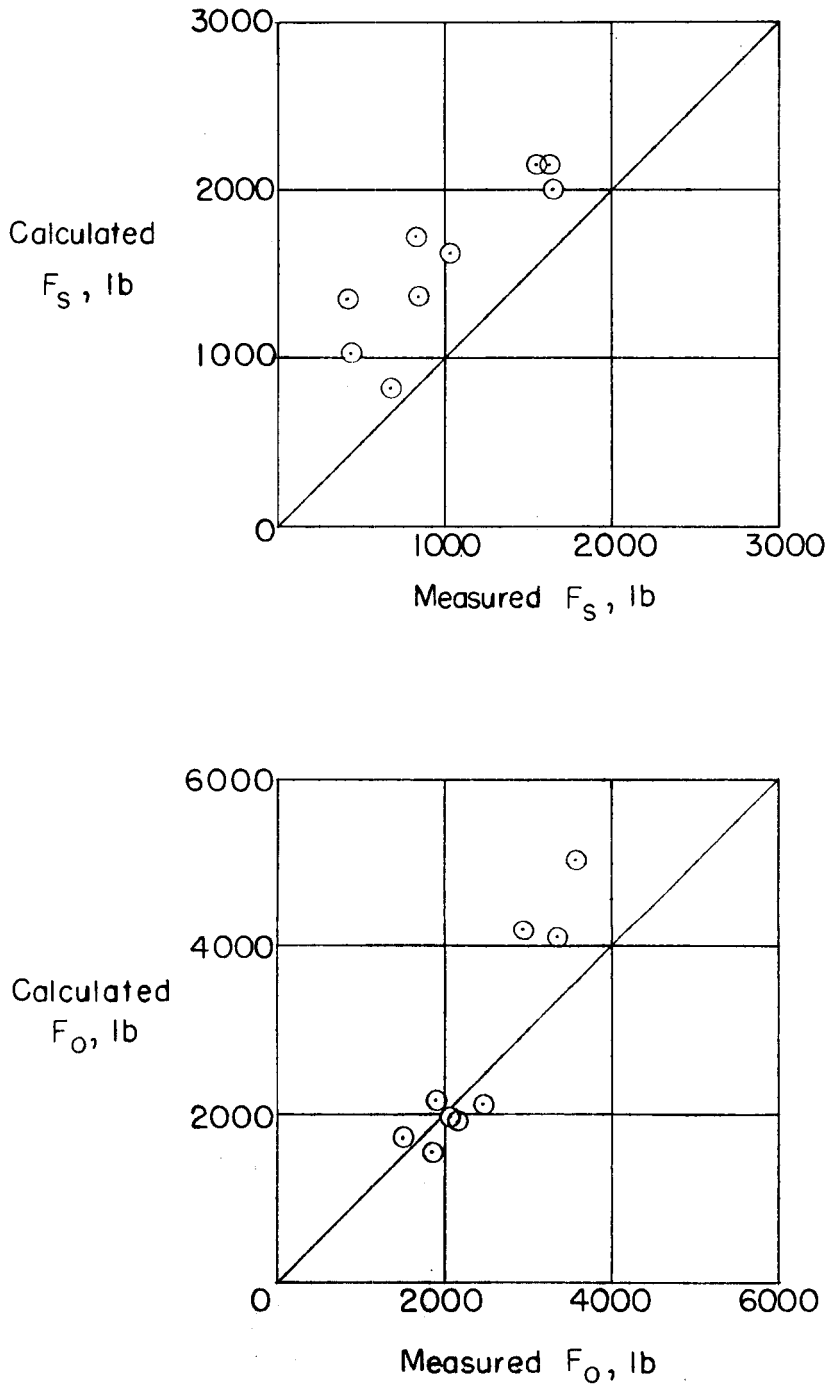

Figure 11.- Comparison of measured and calculated snatch forces and opening shocks. Forces calculated by using the methods suggested in reference 8.

NASA - Langley Field, Va. H-175

A motion-picture film supplement, carrying the same classification as the report, is available on loan. Requests will be filled in the order received. You will be notified of the approximate date scheduled.

The film (16 mm, 20 min, color, silent) shows in-flight deployment and inflation of several test parachutes taken both from the launch aircraft and the parachute test vehicle. The film traces significant steps in the development of the successful drogue parachute for the Project Mercury capsule.

Requests for the film should be addressed to the

National Aeronautics and Space Administration
Office of Technical Information and Educational Programs
Technical Information Division (Code ETV)
Washington 25, D.C.

NOTE: The handling of requests for this classified film will be expedited if application for the loan is made by the individual to whom this copy of the report was issued. In line with established policy, classified material is sent only to previously designated individuals. Your cooperation in this regard will be appreciated.

CONFIDENTIAL

CUT

Date _____

Please send, on loan, copy of film supplement to NASA TM X-448 (Film H-2).

_____

Name of organization

_____

Street number

_____

City and State

Attention:* Mr. _____

Title _____

(*To whom copy No.___ of the Technical Memorandum was issued)